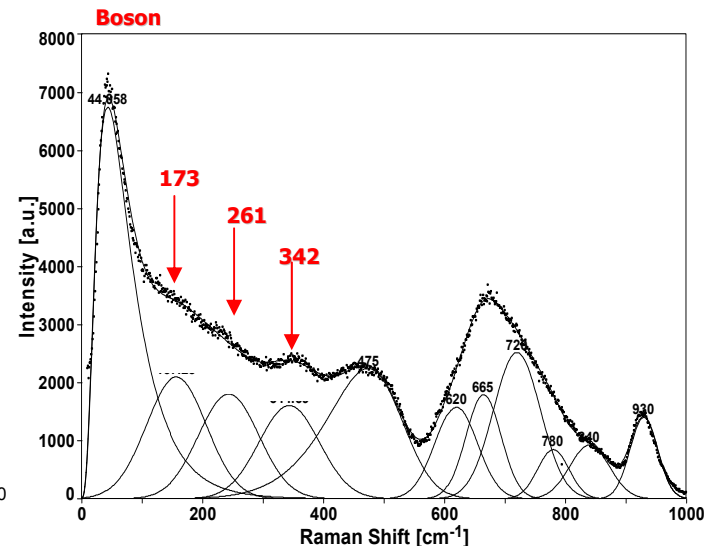
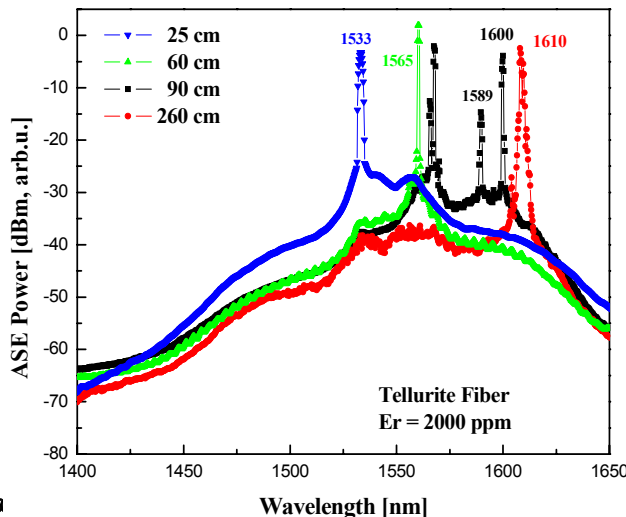
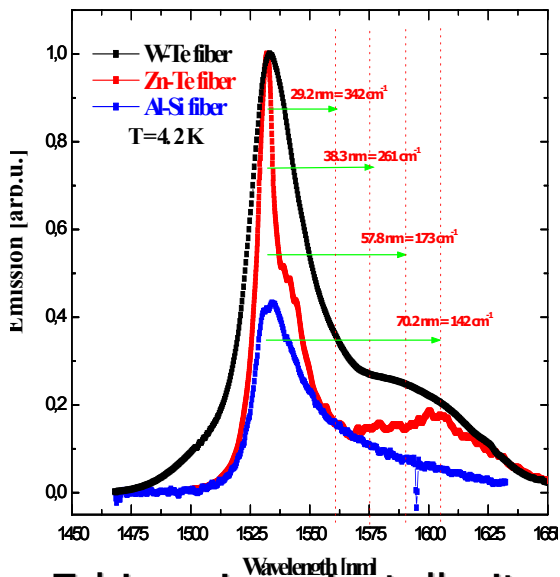




Erbium Emission in Tellurite Glasses and Fibers

J.Toulouse and S.Marjanovic (NSF-DMR Grant #9974031)

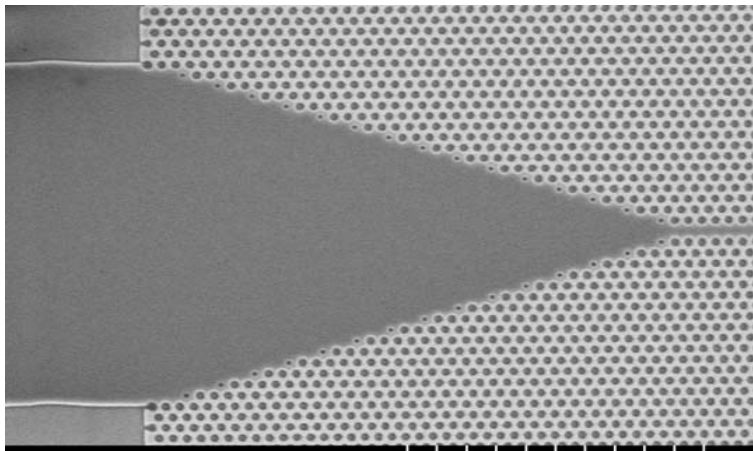


- Erbium ions in tellurite-based glasses emit more strongly than silica, particularly at longer wavelengths (left figure)
- This leads to a very high and flat gain spectrum in fibers (middle figure). The peaks on the broad spectrum are due to resonant transitions between Er energy levels; they appear at longer wavelengths for longer fibers.
- The higher transition efficiencies between Er^{3+} energy levels at longer wavelengths in tellurite glasses are due to phonon-assisted Raman processes (see low frequency phonons indicated by arrows in the Raman spectrum, right, and corresponding arrows on the left figure)
- This effect is further enhanced in fibers due to increased Raman scattering probability and effective re-absorption and re-emission processes.



All-Optical modulation of Si photonic crystals

J. Toulouse and F. Ndi (NSF-DMR Grant #9974031)

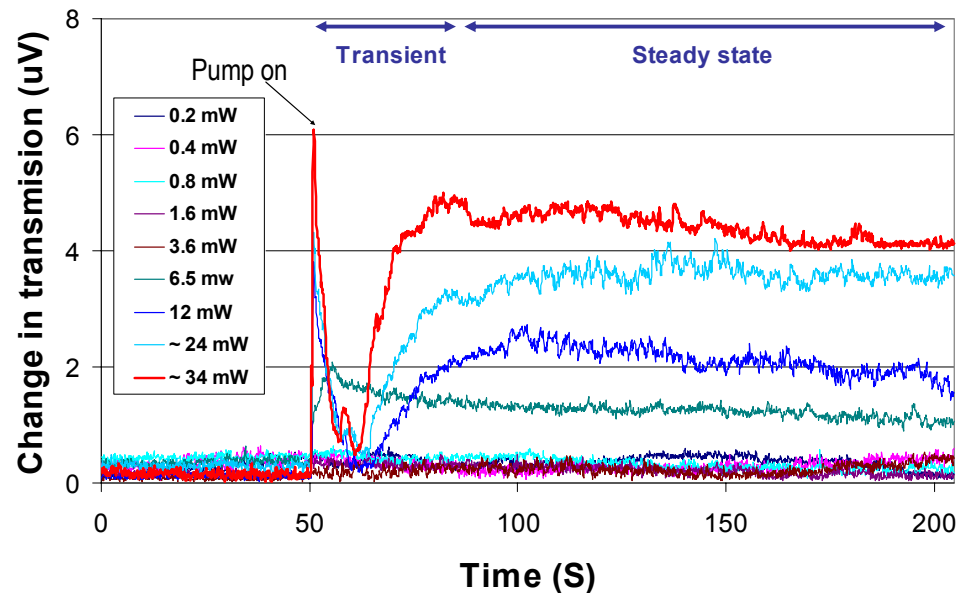


photonic crystal waveguide with taper, hole size $0.38 \mu\text{m}$

- Lattice of air holes in Silicon with lattice spacing on the order of wavelength of light
- Confinement or guidance of light by coherent Bragg reflection

- Optical pumping creates carriers that leads to a change in the refractive index of Silicon and hence a change in the transmission of the waveguide
- Our objective is to achieve all - optical modulation at GHz –frequencies in photonic crystal structures

Change in transmission of 1320nm probe as a function of incident pump power





Nonlinear effects in optical fibers

Jean Toulouse, Iavor Veltchev (NSF-DMR Grant #9974031)

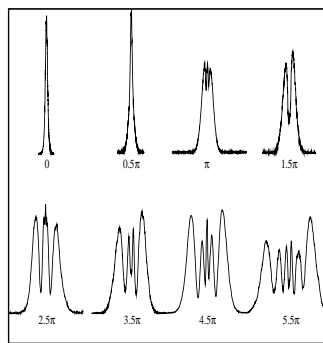
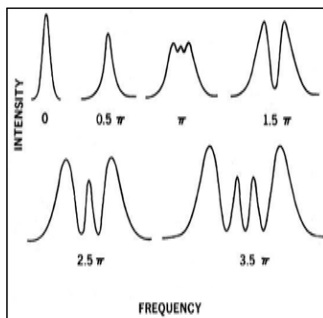
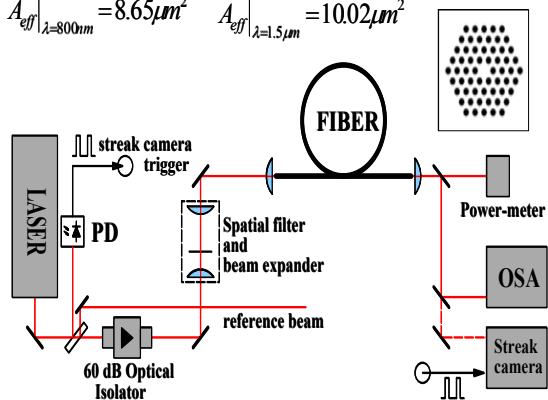
I. Nonlinear index (n_2) of refractive index measurements in optical fiber through Self-Phase Modulation

$$\delta\varphi_{NL} = \frac{2\pi}{\lambda} L_{eff} \delta n_{NL} = \frac{2\pi}{\lambda} \left(\frac{n_2}{A_{eff}} \right) L_{eff} P_m = \gamma L_{eff} P_m; \quad \gamma = \frac{2\pi}{\lambda} \left(\frac{n_2}{A_{eff}} \right)$$

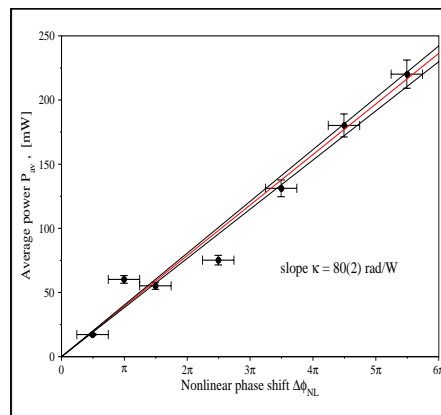
$$A_{eff} = \frac{2\pi \left[\int_0^{\infty} |E(r)|^2 r dr \right]^2}{\int_0^{\infty} |E(r)|^4 r dr} \quad \text{Effective area} \quad L_{eff} = \frac{1}{\alpha} (1 - e^{-\alpha L}) \quad \text{Effective length}$$

The effective area for the holey fiber (hole diameter 1.9 μm , pitch 3.0 μm) is determined through numerical modeling.

$$A_{eff}|_{\lambda=800\text{nm}} = 8.65 \mu\text{m}^2 \quad A_{eff}|_{\lambda=1.5\mu\text{m}} = 10.02 \mu\text{m}^2$$



Experiment



We measure the average laser power for every stage of the self-phase modulation process (nonlinear phase shift). Obviously, the data points at π and 2.5π are incorrectly identified and are excluded from the analysis. Knowledge of the pulse duration, shape, and repetition rate is required in order to obtain the peak power values.

Gaussian pulse: $P_{av} = \frac{\tau f}{2} \sqrt{\frac{\pi}{\ln 2}} P_m$

Sech² pulse: $P_{av} = \frac{\tau f}{0.88} P_m$

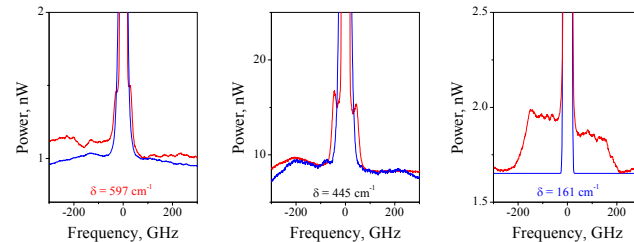
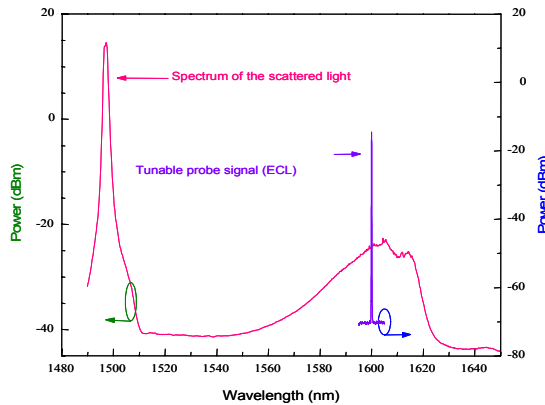
$$\Delta\varphi_{NL} = \frac{\gamma L_{eff}}{\tau f} 0.88 P_{av} \Rightarrow \gamma = \frac{\kappa \tau f}{0.88 L_{eff}} \left\{ \begin{array}{l} \tau = 2.76(3) \text{ ps} \\ f = 76.13(1) \text{ MHz} \\ \kappa = 80(2) \text{ W}^{-1} \\ L_{eff} = 90(1) \text{ cm} \end{array} \right\} = 21.2 \pm 0.6 \text{ W}^{-1} \text{ km}^{-1}$$

$$n_2 = \frac{\gamma \lambda}{2\pi} A_{eff} = 2.33(7) \times 10^{-16} \text{ cm}^2 / \text{W}$$



II. Modulation instability in Raman fiber amplifiers

The coupling between two optical waves in a nonlinear medium leads to a wide variety of fascinating effects. Distributed Raman amplification (DRA), four-wave mixing (FWM), and modulation instability (MI) are the most important ones with implications on the fiber communication systems. DRA is particularly attractive amplification process for use in the fiber-based communication systems. It employs the Raman scattering (light scattering from molecular vibrations) in the same fiber, used for the transmission of data. The wide amplification range (see Fig.1 and Fig.3), fast time response (tens of femtoseconds), and high gain are the most important characteristics of DRA.



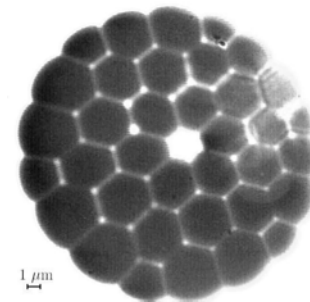
Broadened spectra after Raman amplification in 25 km of Allwave fiber (red) and 20 km of Truewave fiber (blue) for three probe frequency offsets. Sideband frequency shift Δ depends on the probe frequency offset d . No sideband observed in the case of Truewave fiber, as well as in backward-pumping scheme.

We investigate the development of modulation instability in Raman fiber amplifiers. The frequency dependence of the experimentally observed spectral broadening reveals the influence of the two-beam coupling, resulting from the time-delayed Raman part of the third-order nonlinear susceptibility.

III. Supercontinuum generation in microstructured fibers

Supercontinuum generation is achieved in a highly nonlinear microstructured fiber. The two dominant processes leading to the significant spectral broadening are Raman scattering and four-wave mixing. The former transfers energy further into the infrared, whereas the latter process is responsible for mixing the newly created frequency components with the laser frequency to produce new visible frequencies. The supercontinuum spectrum spans the wavelength range (400 – 1400) nm.

Photonic Crystal Fiber (U.Bath)



The supercontinuum spectrum dispersed by a grating and observed by a video camera. The cut-off at ~1000 nm is due to the spectral response of the CCD camera.

